Ultrasonics 93 (2019) 93–101

Contents lists available at ScienceDirect

Ultrasonics

journal homepage: www.elsevier.com/locate/ultras

High-power piezoelectric vibration model considering the interaction between nonlinear vibration and temperature increase

Susumu Miyake*, Ryohei Ozaki, Hiroshi Hosaka, Takeshi Morita

Graduate School of Frontier Sciences, The University of Tokyo, 5-1-5 Kashiwanoha, Kashiwa, Chiba 277-8563, Japan

ARTICLE INFO

Keywords:
Nonlinear piezoelectric vibration
Temperature increase
High-power piezoelectric device
Transfer matrix method
Higher-order elasticity

ABSTRACT

For high-power piezoelectric devices, nonlinear vibrations and related increases in temperature are critical problems produced by large internal stress and strain. Such nonlinear vibrations have been studied by some researchers; however, the related increase in temperature has not been taken into consideration, because it is a complicated phenomenon. In this study, the mechanism underlying the interaction between nonlinear vibration and temperature increase in a piezoelectric transducer under high-power conditions was clarified. For this purpose, cubic terms of the mechanical strain, the nonlinear transfer matrix method, and the heat conduction equation were combined. Additionally, it is necessary to utilize the distributed parameter model because the temperature increase is not uniform. The calculation results obtained using the measured temperature dependence of material constants verified that the temperature increase significantly degrades the piezoelectric vibration. It is expected that the proposed model will prove indispensable in the development of piezoelectric materials for high-power piezoelectric devices.

1. Introduction

Piezoelectric transducers are indispensable in the generation of the high mechanical power required for such applications as medical ultrasonic devices, ultrasonic machining, and ultrasonic motors. High-power operation produces nonlinear piezoelectric vibrations and an increase in temperature, which limit the maximum output power. In the design of such devices, it is essential to estimate the nonlinear characteristics of these piezoelectric vibrations, including the temperature effect. Nonlinear piezoelectric vibrations have substantial effects, including deforming the admittance curve and inducing a hysteretic jump in the current at resonance during frequency sweeping [1–3]. In addition, such nonlinear vibrations cause the temperature to increase and take on a nonuniform spatial distribution. This temperature effect degrades the mechanical quality factor Q_m and changes material constants [4,5].

The difficulty in addressing this problem is that nonlinear vibration and the associated increase in temperature are simultaneous phenomena. In addition, the temperature takes on a nonuniform spatial distribution because the amount of heat generated by the piezoelectric element depends on the internal strain. Therefore, in previous studies, the nonlinear characteristics of piezoelectric elements have been observed using short-term measurements to eliminate the influence of the increase in temperature; two examples of such short-term measurement methods are the burst-mode measurement technique [6–10] and rapid measurement of the admittance curve [11,12]. These previous studies have revealed that higher-order elasticity is the dominant source of nonlinear vibrations and other parameters such as the permittivity and piezoelectric constants can be considered as linear. Therefore, a simple model can be used to evaluate nonlinear piezoelectric vibration under a uniform temperature. As a next step, the actual piezoelectric vibration state including the temperature effect is essential for understanding high-power piezoelectric vibration.

This paper proposes a high-power piezoelectric vibration model including the temperature effect. To calculate the nonlinear vibration and the temperature increase together, a nonlinear transfer matrix method that includes the higher-order complex elasticity was developed and combined with the heat conduction equation. This model was used to simulate the vibration state of a plate-type lead zirconate titanate (PZT) transducer as a fundamental examination. The simulation results were found to agree with the measurement results, demonstrating that the temperature effect enhances nonlinear vibrations and leads to saturation of the vibration velocity. The present results indicate that taking into account the influence of the temperature increase is essential for the functionality of practical devices.

* Corresponding author.
E-mail address: miyake@ems.k.u-tokyo.ac.jp (S. Miyake).

https://doi.org/10.1016/j.ultras.2018.10.014
Received 8 November 2017; Received in revised form 10 August 2018; Accepted 29 October 2018
Available online 03 November 2018
0041-624X/ © 2018 Elsevier B.V. All rights reserved.

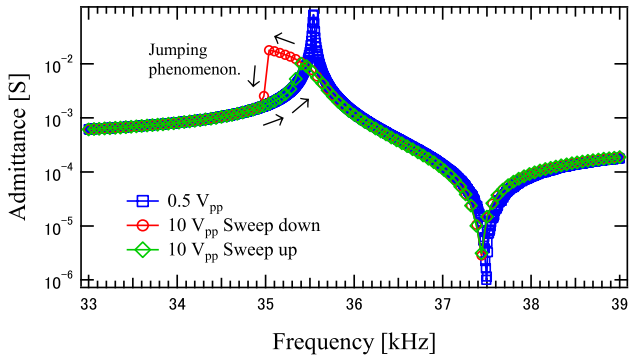

Fig. 1. Admittance curves under low (0.5 V_{pp}) and high (10 V_{pp}) voltages.

2. Nonlinear vibration model

2.1. Lumped parameter model

The admittance curves for a PZT transducer (PZT C-203, 44 mm * 7 mm * 2 mm, Fuji Ceramics) measured for input voltages of 0.5 and 10 V_{pp} are shown in Fig. 1. The schematic diagram of measurement equipment and PZT transducer are shown in Fig. 2. For a low input voltage (0.5 V_{pp}), the admittance curve is symmetric about the resonance frequency; however, under a high input voltage (10 V_{pp}), the admittance curve is deformed, and hysteresis between the upward and downward sweeps and a jumping phenomenon are observed. These characteristics cannot be estimated without considering nonlinear vibrations.

To analyze the piezoelectric vibration, an *LCR* equivalent circuit like the one shown in Fig. 3 is generally used. It is composed of a mechanical *LCR* branch, a force factor A, and a dumped capacitor C_d. The relationship between the motional current i_m and the input voltage V is given as

$$L\frac{\mathrm{d}i_m}{\mathrm{d}t} + Ri_m + \frac{1}{C}\int i_m \mathrm{d}t = V, \tag{1}$$

It has been shown that mechanical nonlinearity is the dominant source of nonlinear piezoelectric vibrations under high-power conditions [11,12]. In this phenomenon, the fundamental vibration mode is affected by a higher vibration mode that is excited by the driving voltage. To estimate the effect of this phenomenon, the equivalent circuit model was improved. The introduction of mechanical nonlinearities with coefficients η and ξ into the mechanical compliance C and the mechanical loss R, respectively, modifies the relationship between i_m and V as

$$L\frac{\mathrm{d}i_m}{\mathrm{d}t} + Ri_m + \eta i_m^3 + \frac{1}{C}\int i_m \mathrm{d}t + \xi\omega^3\left(\int i_m \mathrm{d}t\right)^3 = V. \tag{2}$$

where ω is the angular driving frequency. The nonlinear components ηi_m^3 and $\xi\omega^3(\int i_m dt)^3$ represent the nonlinear mechanical loss and the nonlinear mechanical compliance, respectively. The nonlinear vibrations can be estimated from this equation, and the calculation results have been shown to agree well with experimental results obtained in previous studies [11,12]. However, in these studies, the temperature effect was neglected in the simulation and the experiments.

2.2. Distributed parameter model using a transfer matrix

The nonlinear *LCR* equivalent circuit for the transducer is applicable only at uniform temperatures. In the case of a nonuniform temperature distribution, the material constants become a function of the temperature at each position. To calculate the nonlinear vibration with the temperature effect, the parameter distribution has to be considered. Therefore, a nonlinear transfer matrix was developed by introducing a nonlinear component into the distributed parameter model in a different manner from that in the *LCR* lumped equivalent circuit. To model the mechanical nonlinear effect, the relationship between the strain $\frac{\partial u}{\partial x}$ and stress T_1 is expressed as

$$T_1 = E_1\frac{\partial u}{\partial x} + E_3\left(\frac{\partial u}{\partial x}\right)^3, \tag{3}$$

where E_1 is Young's modulus and E_3 is a nonlinear coefficient. These parameters are defined as complex numbers $E_1 = E_{1r} + jE_{1i}$ and $E_3 = E_{3r} + jE_{3i}$ to express the mechanical loss. The displacement u is given as

$$u = u_0\sin(kx)e^{j(\omega t+\theta)}, \tag{4}$$

where u_0 is the amplitude of the vibration at position x, k is the wave number, and θ is the phase shift of the input voltage. The nonlinear term $E_3\left(\frac{\partial u}{\partial x}\right)^3$ in Eq. (3) produces a third vibration mode. From this term and the identities $\cos^3\omega t = \frac{3}{4}\cos\omega t + \frac{1}{4}\cos 3\omega t$ and $\sin^3\omega t = \frac{3}{4}\sin\omega t - \frac{1}{4}\sin 3\omega t$, the stress component T_ω at the driving angular frequency ω can be expressed as

$$\begin{aligned} T_\omega &= E_1\frac{\partial u}{\partial x} + \frac{3}{4}E_3\left(\frac{\partial u_0\sin(kx)}{\partial x}\right)^3 e^{j(\omega t+\theta)} \\ &= \left\{E_1 + \frac{3}{4}E_3\left(\frac{\partial u_0\sin(kx)}{\partial x}\right)^2\right\}\frac{\partial u}{\partial x} = E'\frac{\partial u}{\partial x}. \end{aligned} \tag{5}$$

From Eq. (5), the nonlinear Young's modulus E' is defined as $E' = E_1 + \frac{3}{4}E_3\left(\frac{\partial u_0\sin(kx)}{\partial x}\right)^2$. This indicates that the apparent Young's modulus of the fundamental vibration depends on the internal stress.

A schematic of the transfer matrix calculation is shown in Fig. 4 [13]. In this calculation method, the transducer is divided into 100 parts, and the force and velocity at each surface are calculated iteratively. The conventional transfer matrix for piezoelectric-31 mode vibrations is expressed as

$$\begin{pmatrix} F_1 \\ v_1 \\ V_0 \\ I_1 \end{pmatrix} = \begin{pmatrix} a & -\frac{SZ}{j}b & (1-a)A & 0 \\ -\frac{b}{jSZ} & a & \frac{b}{jSZ}A & 0 \\ 0 & 0 & 1 & 0 \\ \frac{b}{jSZ}A & (1-a)A & j\omega C_d - \frac{b}{jSZ}A^2 & 1 \end{pmatrix}\begin{pmatrix} F_2 \\ v_2 \\ V_0 \\ I_2 \end{pmatrix} \tag{6}$$

where w, h, ρ, and E are the width, height, density, and Young's modulus for the piezoelectric transducer, respectively; $a = \cos(k\Delta x)$; $b = \sin(k\Delta x)$; Δx is the length of the divided part; $c = \sqrt{\frac{E}{\rho}}$ is the speed of

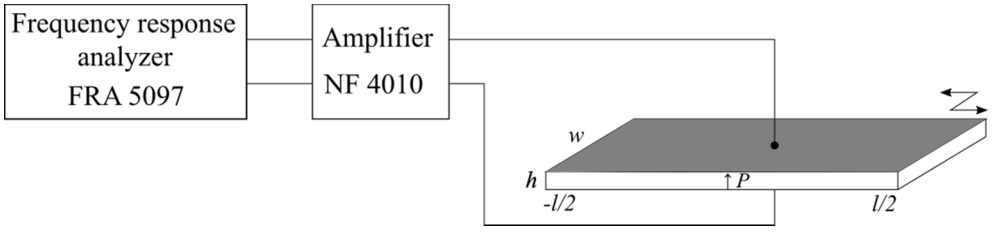

Fig. 2. Schematic diagram of measurement equipment and piezoelectric transducer.

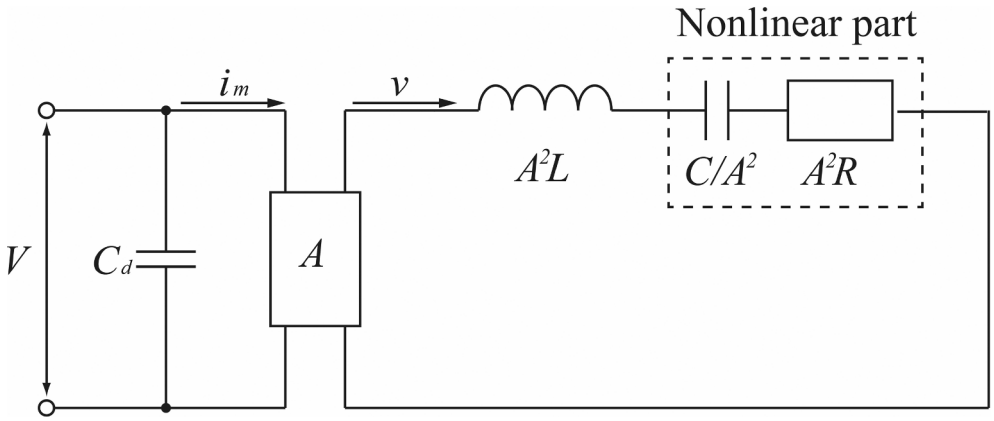

Fig. 3. Piezoelectric *LCR* equivalent circuit: (a) linear model, (b) nonlinear model [11].

sound; $k = \frac{\omega}{c}$ is the wavenumber; $Z = \rho c$ is the characteristic acoustic impedance; $S = wh$ is the cross-sectional area; and $A = \frac{wd_{31}}{s_{11}^E}$ is the force factor, given as a function of the piezoelectric constant d_{31} and the mechanical compliance s_{11}^E. To take the nonlinear effect into account, the nonlinear coefficient E' was used instead of the linear Young's modulus E. Therefore, the speed of sound, the wavenumber, and the characteristic acoustic impedance contain nonlinearities because they depend on the Young's modulus.

As shown in Eq. (5), the nonlinear Young's modulus E' is a function of the strain $\frac{\partial u_0 \sin(kx)}{\partial x}$, and the strain is calculated using the transfer matrix, which includes the Young's modulus E'; therefore, the coefficient E' in the transfer matrix is dependent on the strain distribution. This means that the Young's modulus and strain must be calculated using an iterative calculation algorithm until a steady-state solution is obtained. This calculation algorithm is explained in detail in Section 4. In addition, it is necessary to calculate the temperature distribution to take the temperature effect into account. The method of calculating the temperature is explained in Section 3.

2.3. Relationship between the lumped and distributed parameter models

Under uniform temperature conditions, the nonlinear coefficients ξ and η in the *LCR* model are related to the nonlinear coefficient $E_3 = E_{3r} + jE_{3i}$ in the transfer matrix model; this relationship can be obtained by comparing the nonlinear elastic energy and the nonlinear energy loss in the two models. The nonlinear components of the elastic energies U_l and U_d in the lumped and distributed parameter systems, respectively, are given by

$$U_l = \frac{1}{2}K_{3l}u^2 \tag{7}$$

$$U_d = \frac{1}{2}K_{3d}u^2, \tag{8}$$

where

$$K_{3l} = \frac{whl}{2c^2}\left(\frac{A^2\xi}{2L}v_0^2\right)^2 E_{1r} \tag{9}$$

$$K_{3d} = \frac{9}{32}whlk^4E_{3r}u_0^2. \tag{10}$$

The nonlinear energy loss rates W_l and W_d in the lumped and distributed parameter systems, respectively, are given by

$$W_l = R_{3l}v^2 \tag{11}$$

$$W_d = R_{3d}v^2, \tag{12}$$

where

$$R_{3l} = \frac{A^2m\eta}{L}v_0^2 \tag{13}$$

$$R_{3d} = \frac{9}{32}\frac{whlk^4E_{3i}v_0^2}{\omega^3}, \tag{14}$$

v is the vibration velocity, v_0 is the amplitude of the velocity, and m is the equivalent mass of the transducer. From the relationships $U_l = U_d$ and $W_l = W_d$ and Eqs. (9)–(14), the relationship between the nonlinear coefficients can be obtained as

$$\begin{pmatrix} F_0 \\ v_0 \\ V_0 \\ I_1 \end{pmatrix} = \begin{pmatrix} \cos(kl) & -\frac{SZ_0}{j}\sin(kl) & (1-\cos(kl))A & 0 \\ -\frac{\sin(kl)}{jSZ_0} & \cos(kl) & \frac{\sin(kl)}{jSZ_0}A & 0 \\ 0 & 0 & 1 & 0 \\ \frac{\sin(kl)}{jSZ_0}A & (1-\cos(kl))A & j\omega C_d - \frac{\sin(kl)}{jSZ_0}A^2 & 1 \end{pmatrix} \begin{pmatrix} F_1 \\ v_1 \\ V_0 \\ I_2 \end{pmatrix}$$

$$\begin{pmatrix} F_1 \\ v_1 \\ V_0 \\ I_2 \end{pmatrix} = \begin{pmatrix} \cos(kl) & -\frac{SZ_0}{j}\sin(kl) & (1-\cos(kl))A & 0 \\ -\frac{\sin(kl)}{jSZ_0} & \cos(kl) & \frac{\sin(kl)}{jSZ_0}A & 0 \\ 0 & 0 & 1 & 0 \\ \frac{\sin(kl)}{jSZ_0}A & (1-\cos(kl))A & j\omega C_d - \frac{\sin(kl)}{jSZ_0}A^2 & 1 \end{pmatrix} \begin{pmatrix} F_2 \\ v_2 \\ V_0 \\ I_3 \end{pmatrix}$$

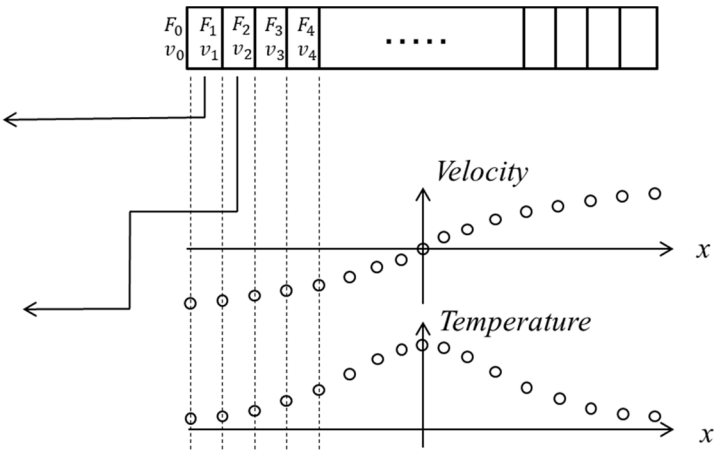

Fig. 4. Schematic of transfer matrix calculation.

$$E_{3r} = \frac{16}{9}\frac{E_{1r}^2 A^2}{\rho\omega L}\xi \tag{15}$$

$$E_{3i} = \frac{16}{9}\frac{E_{1r}^2 A^2}{\rho\omega L}\eta. \tag{16}$$

With these equations, the nonlinear coefficients E_{3r} and E_{3i} can be calculated from ξ, η, and the linear material constants. In this study, ξ and η were obtained by admittance curve fitting using the *LCR* equivalent circuit [11,12]. The force factor A, density ρ, and circuit constant L were also obtained from this measurement. The real part of the linear Young's modulus E_{1r} can be calculated as

$$E_{1r} = \frac{1}{s_{11}^E}, \tag{17}$$

where the linear mechanical compliance s_{11}^E is related to the circuit constants of the *LCR* equivalent circuit as

$$s_{11}^E = \frac{\pi^2 whC}{2lA^2}. \tag{18}$$

3. Temperature distribution model

In the proposed calculation model, the transducer is divided into 100 parts in the longitudinal direction. The vibration velocity and the temperature distribution can be calculated from the material constants obtained as a function of the temperature at each division. To calculate the temperature distribution in a rectangular plate-type piezoelectric transducer, the one-dimensional steady-state heat conduction equation is adopted as

$$\frac{\partial T}{\partial t} = 0 = \lambda wh\frac{\partial^2 T}{\partial x^2} + \dot{q} - 2\alpha wh(T - T_\infty), \tag{19}$$

where T is the temperature, λ is the thermal conductivity, α is the convective heat transfer coefficient, T_∞ is the atmospheric temperature, and $\dot{q}$ is the heat generation rate. In this study, λ was set to 1.5 W/(m K) and α was measured as 17.9 W/(m^2 K). The heat generation rate $\dot{q}$ was obtained from the mechanical energy loss including the nonlinear piezoelectric vibration as

$$\dot{q} = \frac{1}{2}\frac{whE_{1i}}{\omega}\left(\frac{\partial v_x}{\partial x}\right)^2 + \frac{3}{8}\frac{whE_{3i}}{\omega^3}\left(\frac{\partial v_x}{\partial x}\right)^4, \tag{20}$$

where $v_x = v_0\sin(kx)$. The heat generation rate $\dot{q}$ depends on v_x, as shown in Eq. (20). In contrast, the temperature affects the material constants, and this in turn modifies the vibration mode. To obtain a steady-state solution for the vibration mode and the temperature distribution, an iterative calculation using the nonlinear transfer matrix and the heat conduction equation is required.

4. Calculation algorithm

The nonlinear vibration mode including the temperature effect was solved by combining the nonlinear transfer matrix and the heat conduction equation. For this calculation, an iterative process is necessary because two loop relationships are involved. The first is the relationship between the vibration mode and the nonlinear Young's modulus E', as described by Eqs. (5) and (6), and the second is that between the vibration mode and the temperature distribution, as described by Eqs. (5), (6), (19), and (20). This iterative calculation algorithm is shown in Fig. 5. After the vibration mode has been obtained by iteratively solving Eqs. (5) and (6), the heat generation rate is calculated from Eq. (18), enabling the calculation of the temperature distribution using the vibration mode and Eq. (17). At this point, the material constants have been altered slightly by the temperature distribution. This necessitates continuous calculation of the vibration velocity using the updated material constants. The calculation is repeated until a steady state has been reached. To realize this calculation process, the material constants should be measured in advance as functions of temperature, as explained in the next section.

5. Measurement of temperature-dependent material constants

5.1. Measurement method

The temperature dependence of the material constants is required for the nonlinear vibration calculation explained in Section 4. The temperature-dependent material constants for a piezoelectric transducer were obtained by measuring its admittance curve. Fig. 6 shows the experimental setup. A rectangular plate-type PZT transducer (PZT C-203, 44 mm * 7 mm * 2 mm, Fuji Ceramics) was used in this study. The transducer was placed in a thermostat chamber (DKN302, Yamato Scientific Co., Ltd.). To measure the material constants, a frequency response analyzer (FRA5097, NF Corporation) was used in conjunction with a power amplifier (4010, NF Corporation). The temperature distribution was kept uniform during the admittance curve measurement, and the ambient temperature was set to 28, 35, 40, 50, and 60 °C by the thermostat chamber for each measurement. After the ambient temperature was changed, the transducer was not operated until its temperature became uniform. In addition, the admittance curve was measured over a short period to ensure the temperature at the center did not increase. The allowable measurement time depends on the input voltage. In the present measurements, the admittance curves were measured for 30 and 3 s for the input voltages of 0.5 V_{pp} and 10 V_{pp}, respectively.

Admittance curves measured under the low input voltage (0.5 V_{pp}) reflect conditions with sufficiently low stress inside the material and a low nonlinear effect. The temperature-dependent material constants were obtained by fitting the admittance curve for the equivalent circuit shown in Fig. 3(a) to the measured admittance curves under various temperature conditions at this input voltage. The admittance is expressed as

$$Y = \frac{1}{j\omega L + \frac{1}{j\omega C} + R} + j\omega C_d. \tag{21}$$

In addition, the admittance curves were measured under the high input voltage (10 V_{pp}). The nonlinear coefficients ξ and η were obtained from these high-voltage measurements through curve fitting using the equivalent circuit shown in Fig. 3(b). The relationship between the motional current i_m and the input voltage V is given by Eq. (2). Substituting $V = V_0\cos\omega t$ and $i_m = i_0\cos(\omega t + \theta)$ into Eq. (2) yields the following relationship between i_0 and V_0: [11]

$$\left(-\omega L i_0 + \frac{i_0}{\omega C_0} + \frac{3}{4}\xi i_0^3\right)^2 + \left(R_0 i_0 + \frac{3}{4}\eta i_0^3\right)^2 = V_0^2. \tag{22}$$

The phase shift θ was calculated as [11]

$$\theta = \tan^{-1}\frac{-\omega L + \frac{1}{\omega C_0} + \frac{3}{4}\xi i_0^2}{R_0 + \frac{3}{4}\eta i_0^2}. \tag{23}$$

From this, the admittance was calculated as

$$Y = \frac{i_0}{V_0}\cos\theta + j\frac{i_0}{V_0}\sin\theta + j\omega C_d. \tag{24}$$

During this curve fitting, the equivalent mass L, the mechanical compliance C, and the mechanical loss R were fixed to the values obtained from the curve fitting of the measurement results with 0.5 V_{pp}. The nonlinear coefficients E_{3r} and E_{3i} were calculated from ξ and η using Eqs. (15) and (16).

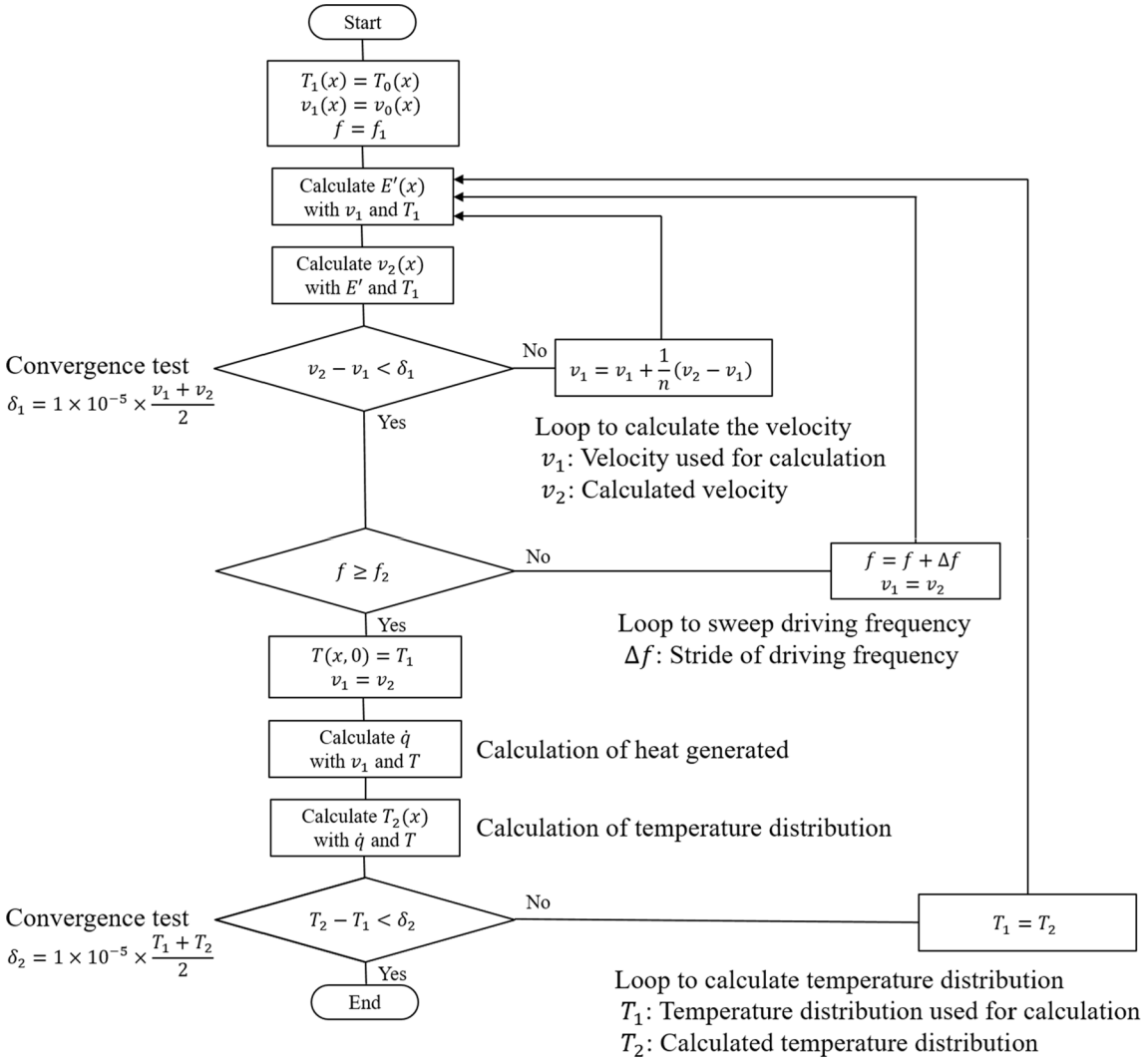

Fig. 5. Flowchart for calculating nonlinear vibration with temperature effect.

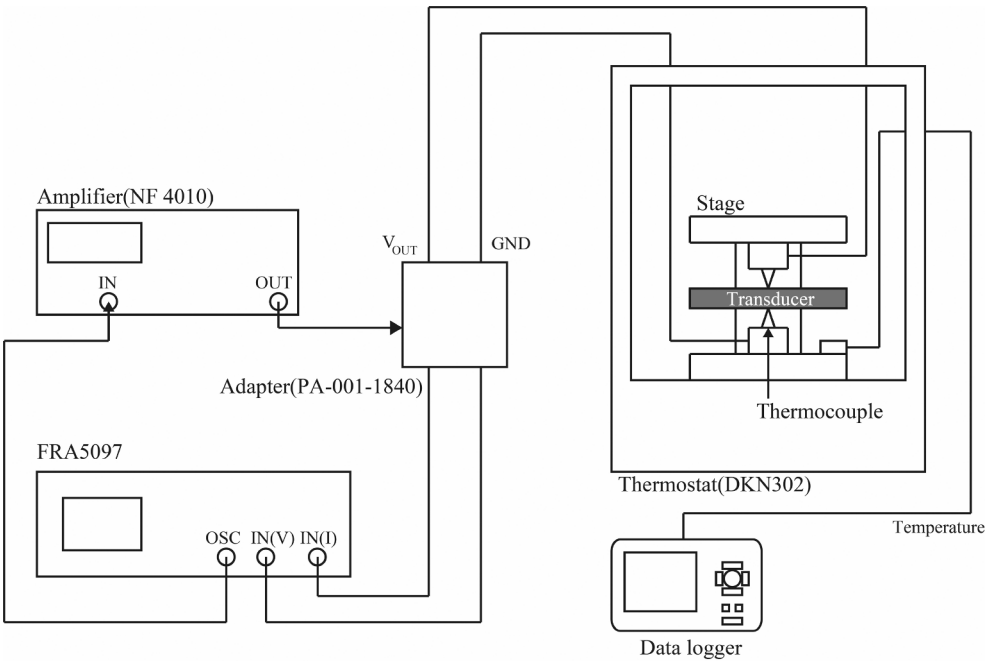

Fig. 6. Experimental setup for measurement of temperature-dependent material constants.

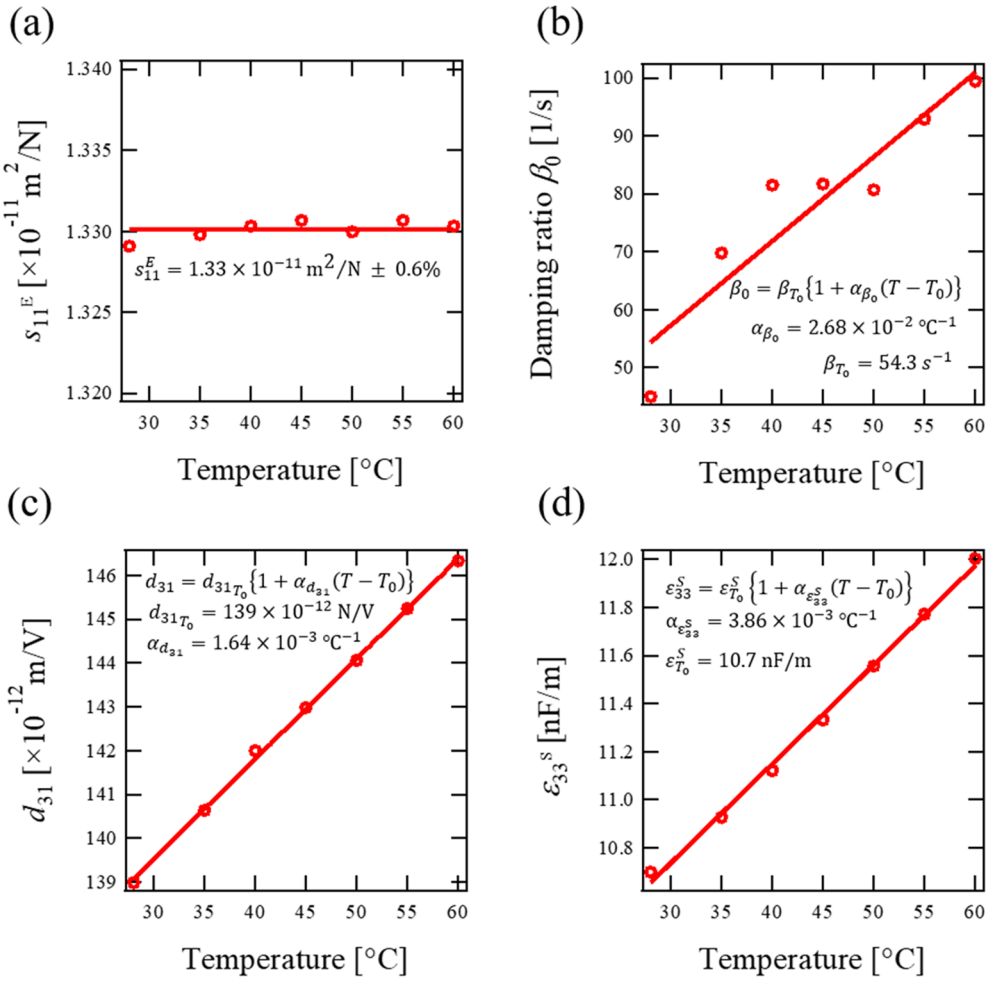

Fig. 7. Temperature dependence of material constants measured with input voltage of 0.5 V_{pp}: (a) compliance, (b) damping ratio, (c) piezoelectric constant, and (d) dielectric coefficient.

5.2. Results

From the curve fitting of the low-voltage measurement results, the temperature dependence of the compliance s_{11}^E, damping ratioβ_0, dielectric constant $\varepsilon_{33}{}^S$, and piezoelectric constant d_{31} was obtained, as shown in Fig. 7. The damping ratio is related to the mechanical loss of the vibration and was calculated as

$$\beta_0 = \frac{R_0}{2m}. \tag{25}$$

The compliance s_{11}^E can be regarded as constant and was found to be within 1.33×10^{-11}m^2/N ± 0.6%. Linear equations were used to approximate β_0, $\varepsilon_{33}{}^S$, and d_{31} at room temperature (T_0 = 28Â°C), as shown in Fig. 7. Fig. 8 shows the temperature dependence of the nonlinear coefficients. The nonlinear coefficient E_{3r}, which is related to the mechanical stiffness, decreased with increasing temperature. This indicates that increasing temperature causes the resonance frequency to decrease. The nonlinear coefficient E_{3i} is related to the mechanical loss and increases with increasing temperature. This means that increasing temperature results in a larger vibration loss and further heat generation. These material properties were utilized in the calculation model described in Section 4.

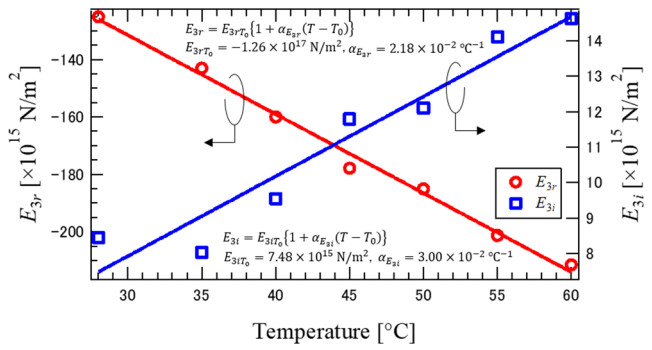

Fig. 8. Temperature dependence of nonlinear coefficients.

6. Simulation

6.1. Admittance curve

Using the model described in Section 4, the admittance curve including the temperature effect was calculated. An example of the calculated admittance curves with an input voltage of 30 V_{pp} is shown in Fig. 9. Calculations were conducted both allowing for and neglecting the temperature distribution. Both cases show hysteresis in the admittance curve with respect to the driving frequency, which is due to the nonlinear effect. With the temperature distribution taken into consideration, the maximum admittance at the resonance frequency decreases by 37% and the downward jump frequency increases by 480 Hz relative to those without the temperature effect. In the case of the upward frequency sweep, there is no difference between the calculated admittance curves with and without the temperature distribution. This is because a low vibration velocity does not cause the

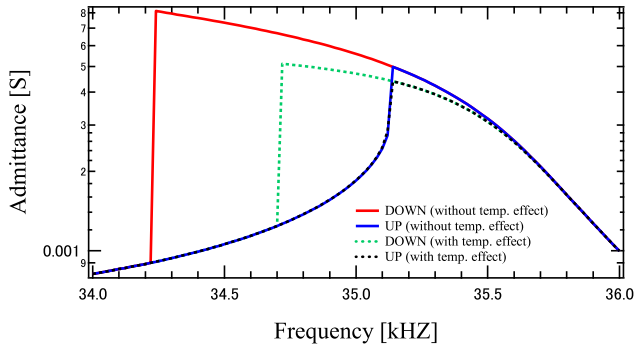

Fig. 9. Calculated admittance curves with and without temperature effect under input voltage of 30 V_{pp}.

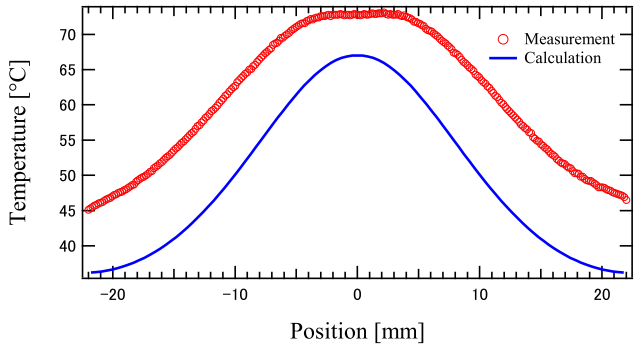

Fig. 10. Calculated and measured temperature distributions under input voltage of 30 V_{pp}.

temperature to increase.

Fig. 10 shows the calculated and measured temperature distributions at an input voltage of 30 V_{pp}. The calculation was conducted with upward and downward frequency sweeps. The surface temperature distribution was obtained using an infrared thermal camera (InfReC F30W, Nippon Avonics Co., Ltd.) during the downward frequency sweep. During the downward sweep, the calculated temperature at the center of the transducer reaches 67.0 °C, and the corresponding measured temperature is 73.1 °C. The driving frequency in the measurement and calculation was 34.27 kHz and 34.72 kHz, which maximizes the vibration velocity. The difference between the calculated and measured driving frequencies is caused by characteristic changes to the sample transducer due to the repeated measurement. During the upward sweep, the calculated temperature distribution is almost uniform at room temperature (T = 28 °C) because of the low internal stress and strain.

6.2. Vibration velocity

Under high-power conditions, the nonlinear effect causes a decrease in the maximum vibration velocity. The maximum vibration velocity was calculated as a function of the input voltage using the proposed calculation model. The calculation results for the vibration velocity amplitude and the temperature at the center of the transducer are shown in Fig. 11. Measured results are also shown in the figure. Measurement method and discussion are shown in the next section. The velocity was calculated both allowing for and neglecting the temperature effect. The temperature at the center of the transducer in the case including the temperature effect is also shown in this figure. With increasing input voltage, the temperature of the transducer increases, and the vibration velocity saturates. As a result, the vibration velocity is reduced by 33.9% at an input voltage of 30V_{pp} compared to the case with no temperature distribution. When the velocity is saturated, the additional voltage input to the piezoelectric transducer is not converted to mechanical energy but instead leads to heat generation. The saturation velocity is important as an evaluation index in the application of high-power ultrasonic devices.

7. Measurement of vibration velocity saturation

The simulation results indicate that the interaction between the nonlinear vibration and the temperature effect results in the further suppression of the vibration velocity. To demonstrate the applicability of the proposed calculation model, the maximum vibration velocity was measured with and without the temperature effect. To measure the maximum vibration velocity, the driving frequency was swept downward. For this measurement, a function generator (WF1974, NF Corporation), a power amplifier (4010, NF Corporation), and a laser Doppler velocimeter (NLV 2500, Polytec Ltd.) were used, as shown in Fig. 12. The laser was used to irradiate the tip of the transducer to measure the vibration velocity in the longitudinal vibration mode. The transducer was supported at the center by the thermocouple and was driven continuously. The velocity was measured when the temperature reached saturation. The output signal from the laser Doppler velocimeter was input into the lock-in amplifier (LI5660, NF Corporation), and only the vibration velocity signal at the driving frequency was obtained. The equipment was controlled by a personal computer (PC) with a general-purpose interface bus (GPIB) system.

Measurement of the velocity without the temperature effect must be conducted over a short duration. To avoid any increase in the temperature, a burst signal input voltage in the range of 0.1–30 V_{pp} was applied to the transducer for a short duration of 3000 cycles. The nonlinear effect causes the resonance frequency, which produces the maximum vibration velocity, to shift as a function of the driving voltage. The frequency response of the velocity amplitude was measured, and the maximum velocity was obtained at each driving voltage. To measure the maximum vibration velocity, the driving frequency was swept downward because the nonlinear piezoelectric vibration shows hysteresis.

The measured relationship between the velocity amplitude and the temperature with and without the temperature effect is shown in Fig. 11. The measurement results agree with those of the simulation; this demonstrates the validity of the proposed nonlinear model. In both the measurement and simulation results, the velocity with the temperature effect is 30% less than that without. This indicates that the temperature effect results in a serious performance degradation of the transducer. It is because linear and nonlinear vibration loss increase with temperature increase. Increased vibration loss generates more heat and temperature increase. In the practical design of high-power ultrasonic devices, it is essential to consider this interaction because it conditions the maximum vibration velocity, as shown in Fig. 11.

8. Conclusion

In this paper, a model of piezoelectric vibration under high-power conditions was proposed. This model is based on a nonlinear transfer matrix model, and the temperature distribution is taken into consideration using the heat conduction equation. Therefore, nonlinear vibrations and the temperature effect can be calculated together. The temperature dependence of the material constants was measured in advance and used in the calculations. With the proposed model, the high-power characteristics of a PZT transducer were successfully evaluated. The calculation results showed that the interaction between the temperature increase and nonlinear vibrations causes the maximum vibration velocity and the saturation velocity to decrease. Although the PZT transducer has a high mechanical quality factor under a low input voltage, the calculation results indicate that the performance cannot be maintained under high-power conditions. The proposed model realized describing nonlinear effect and temperature effect together. It is the innovative progress for the practical evaluation of the high-power

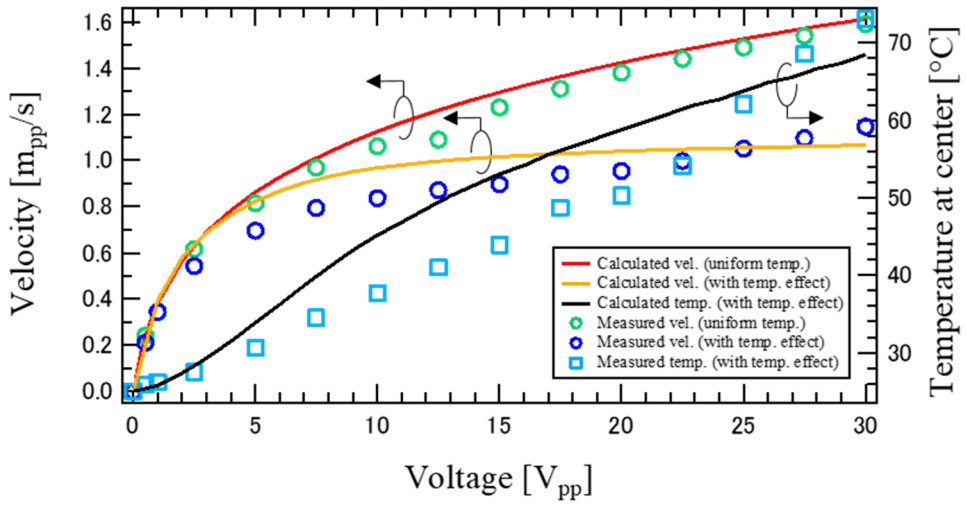

Fig. 11. Calculated and measured velocities and temperatures with and without temperature effect.

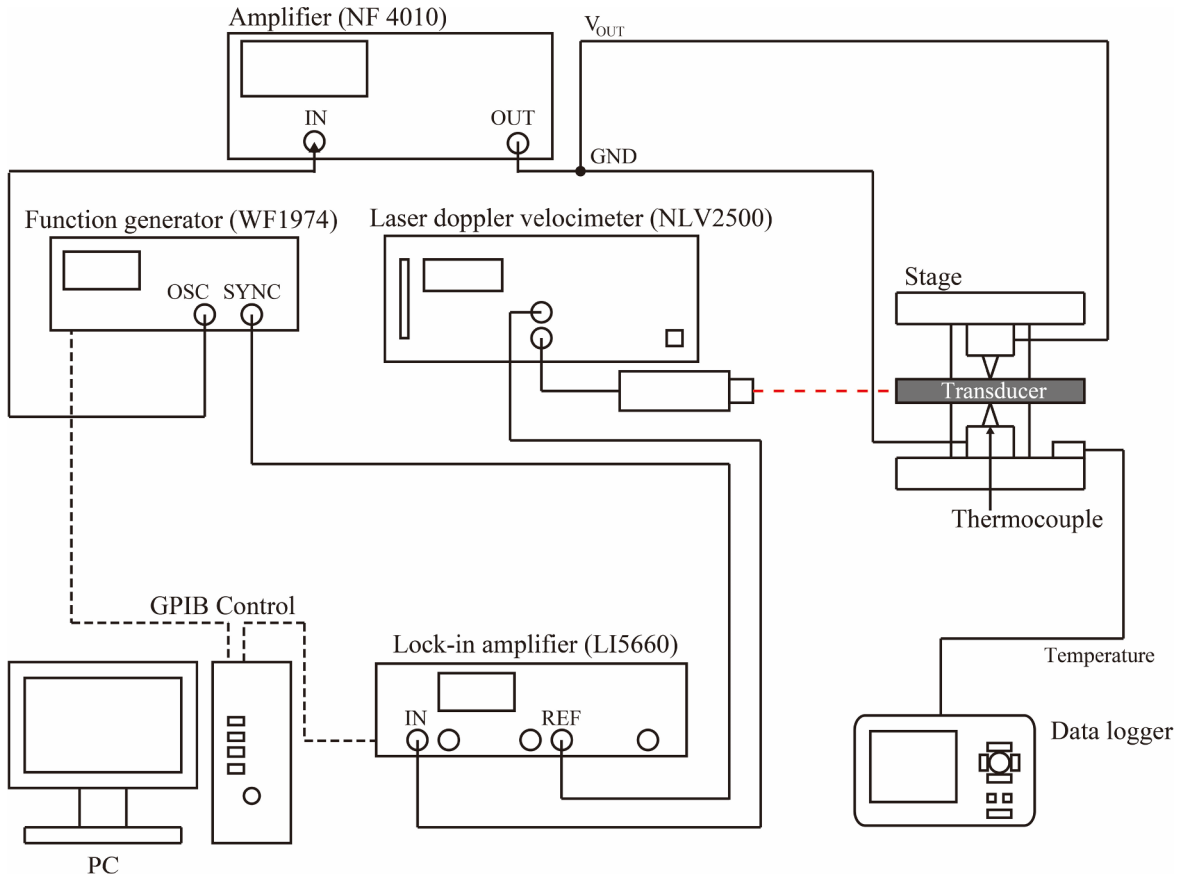

Fig. 12. Measurement system for velocity without temperature effect.

piezoelectric transducer. In future work, the high-power characteristics of various piezoelectric materials will be investigated. The proposed model is expected to prove useful in determining the piezoelectric materials that are best suited for high-power operation.

Acknowledgements

This work was supported by JSPS KAKENHI Grant number 18J22170 and NSK Foundation for the Advancement of Mechatronics.

References

[1] K. Ishii, N. Akimoto, S. Tashiro, H. Igarashi, Jump phenomena of current in piezoelectric ceramic vibrators under high power conditions, J. Eur. Ceram. Soc. 19 (1999) 1157–1160.
[2] C.H. Xu, H.L.W. Chan, Behaviors of piezoelectric vibrators driven by high electric field at the frequencies near resonance, Mater. Chem. Phys. 82 (2003) 758–763.
[3] U.v. Wagner, Nonlinear lingitudinal vibrations of piezoceramics excited by weak electric fields, Int. J. Nonlinear Mech. 38 (2003) 565–574.
[4] S. Tashiro, M. Ikehiro, H. Igarashi, Influence of temperature rise and vibration level on electromechanical properties of high power piezoelectric ceramics, Jpn. J. Appl. Phys. 36 (1997) 3004–3009.

[5] T. Yamamoto, F. Mizuno, Degradation of piezoelectric properties at resonant operational mode by a large input power, Jpn. J. Appl. Phys. 34 (1995) 2627–2631.
[6] K. Uchino, J. Zheng, A. Joshi, Y.H. Chen, S. Yoshikawa, S. Hirose, S. Takahashi, J.W.C. de Vries, High power characterization of piezoelectric materials, J. Electroceram. 2 (1) (1998) 33–40.
[7] A. Albareda, J.A. Casals, R. Perez, F. Montero de Espinosa, Nonlinear measurements of high power 1 3 piezo air transducers with burst excitation, Ferroelectrics 273 (2002) 47–52.
[8] M. Umeda, K. Nakamura, S. Takahashi, S. Ueha, An analysis of jumping and dropping phenomena of piezoelectric transducers using the electrical equivalent circuit constants at high vibration amplitude levels, Jpn. J. Appl. Phys. 39 (2000) 5623–5628.
[9] M. Umeda, K. Nakamura, S. Ueha, Effects of vibration stress and temperature on the characteristics of piezoelectric ceramics under high vibration amplitude levels measured by electrical transient responses, Jpn. J. Appl. Phys. 38 (1999) 5581–5585.
[10] M. Umeda, K. Nakamura, S. Ueha, The measurement of high power characteristics for a piezoelectric transducer based on the electrical transient response, Jpn. J. Appl. Phys. 37 (1998) 5322–5325.
[11] Y. Liu, R. Ozaki, T. Morita, Investigation of nonlinearity in piezoelectric transducers, Sensor. Actuat. A-Phys. 227 (2015) 31–38.
[12] Y. Liu, T. Morita, Simplified determination of nonlinear coefficients in piezoelectric transducers, Jpn. J. Appl. Phys. 54 (2015) 10ND01.
[13] E.K. Sitting, Transmission parameters of thickness-driven piezoelectric transducers arranged in multilayer configurations, IEEE Trans. Sonics. Ultrason. SU-14 (4) (1967) 167–174.